HAL open science

Identification of the three zinc-binding sites on tau protein

Romain Rocca, Philipp O Tsvetkov, Andrey Golovin, Diane Allegro, Pascale Barbier, Soazig Malesinski, Françoise Guerlesquin, François Devred

To cite this version:

Romain Rocca, Philipp O Tsvetkov, Andrey Golovin, Diane Allegro, Pascale Barbier, et al.. Identification of the three zinc-binding sites on tau protein. International Journal of Biological Macromolecules, 2022, 209, pp.779-784. 10.1016/j.ijbiomac.2022.04.058 . hal-03647684

HAL Id: hal-03647684

https://amu.hal.science/hal-03647684v1

Submitted on 29 Apr 2022

HAL is a multi-disciplinary open access archive for the deposit and dissemination of scientific research documents, whether they are published or not. The documents may come from teaching and research institutions in France or abroad, or from public or private research centers.

L'archive ouverte pluridisciplinaire **HAL**, est destinée au dépôt et à la diffusion de documents scientifiques de niveau recherche, publiés ou non, émanant des établissements d'enseignement et de recherche français ou étrangers, des laboratoires publics ou privés.

Identification of the three zinc-binding sites on Tau protein.

Romain La Rocca[1], Philipp O. Tsvetkov[1,2*], Andrey V. Golovin[3,4,5], Diane Allegro[1], Pascale Barbier[1], Soazig Malesinski[1], Françoise Guerlesquin[6], François Devred[1,2*].

[1]Aix Marseille Univ, CNRS, UMR 7051, INP, Inst Neurophysiopathol, Fac Médecine, Marseille, France;

[2]Aix Marseille Univ, CNRS, PINT, Plateforme INteractome Timone, Fac Médecine, Marseille, France;

[3]Bioengineering and Bioinformatics Department, M. V. Lomonosov Moscow State University, Leninskie Gory 1, 119992 Moscow, Russian Federation;

[4] Institute of Molecular Medicine, I.M. Sechenov First Moscow State Medical University, Trubetskaya Str. 8, Moscow, 119992, Russia;

[5] National Research University HSE, Myasnitskaya Str. 20, Moscow, 101000, Russia;

[6] Aix-Marseille Univ, CNRS, UMR 7255, Laboratoire d'Ingénierie des Systèmes Macromoléculaires, Institut de Microbiologie de la Méditerranée, Marseille, France.

* Corresponding authors: francois.devred@univ-amu.fr ; philipp.tsvetkov@univ-amu.fr

Authors e-mail: RLR: romain.la-rocca@univ-amu.fr; POT: philipp.tsvetkov@univ-amu.fr;

AVG: golovin.andrey@gmail.com; DA : diane.allegro@univ-amu.fr; PB:

pascale.barbier@univ-amu.fr; SM : soazig.malesinksi@univ-amu.fr; FG:

guerlesquin@imm.cnrs.fr; FD: francois.devred@univ-amu.fr

Declaration of interest: none.

Funding: This work was partly supported by research funding from the Cancéropôle PACA, Institut National du Cancer and Région Sud.

Highlights:

- Zinc is known to induce tau aggregation in neurodegenerative diseases
- Zinc binding locations and mechanism are not yet clear
- Using NMR we localized 3 zinc binding site on tau
- By molecular simulations, we proposed a modeled structure of each site
- Our findings pave the way for designing potential therapies for tauopathies

Abstract:

Tau protein has been extensively studied due to its key roles in microtubular cytoskeleton regulation and in the formation of aggregates found in some neurodegenerative diseases. Recently it has been shown that zinc is able to induce tau aggregation by interacting with several binding sites. However, the precise location of these sites and the molecular mechanism of zinc-induced aggregation remain unknown. Here we used Nuclear Magnetic Resonance (NMR) to identify zinc binding sites on tau. These experiments revealed three distinct zinc binding sites on tau, located in the N-terminal part, the repeat region and the C-terminal part. Further analysis enabled us to show that the N-terminal and the C-terminal sites are independent of each other. Using molecular simulations, we proposed a model of each site in a complex with zinc. Given the clinical importance of zinc in tau aggregation, our findings pave the way for designing potential therapies for tauopathies.

Keywords: Tau, zinc, binding sites, NMR

1. Introduction

Microtubule-associated protein tau plays a central role in cytoskeleton dynamicity via its regulatory activity on microtubule dynamics, which impacts microtubule functions in various processes such as cell division and axonal stability in neurons [1,2]. In addition, tau has also been shown to be associated with a number of neurodegenerative diseases such as Alzheimer's disease (AD), Parkinson's disease (PD) and frontotemporal lobar degeneration, also called Tauopathies [3–6]. In several Tauopathies, tau forms neurofibrillary tangles, which consist of stacked paired helical filaments (PHF) of hyper-phosphorylated tau molecules [7].

Dyshomeostasis of metal ions, such as iron, copper, zinc and calcium play an important role in the development of neurodegenerative diseases [8]. For example, recent findings demonstrated the catalytic role of copper in tau aggregation [9]. Still zinc, in competition with other ions in its ability to induce the aggregation of proteins involved in neurodegenerative diseases, takes the first place. Indeed, zinc has been identified as a factor favoring the aggregation of amyloid-β [10,11], FUS/TLS [12], TDP-43 [13,14] and tau [15]. Among the endogenous factors that have been shown to favor tau aggregation, zinc seems to play an important role in AD [16]. Zinc has been shown to increase the toxicity of tau in cells [17] mainly through an interaction with tau. More recently, this effect was confirmed in neurons where zinc induces cell death through the acceleration of tau aggregation [18,19]. Several molecular works proved that zinc can also accelerate aggregation of purified tau constructs [15,20,21], thus confirming the direct effect of zinc on tau. In addition, zinc has been recently shown to induce the formation of reversible aggregation of tau [22,23], and to promote Liquid-Liquid Phase Separation (LLPS) of tau [24,25] which could either be part of the early stages of pathological aggregation similarly to tau phosphorylation [26], or a physiological concurrent pathway.

Despite the importance of zinc binding to tau, the exact binding sites are not currently known. Two reports have already addressed this question and spotted seven residues located in the R2-R3 repeat region of tau (C291, C322, H268, H299, H329, H330, and H362) [15,18]. Among these amino acids, the cysteines located in the repeat region of tau (C291 and C322) were identified as the core of the interaction between a tau peptide (244-372) and zinc. Binding of zinc in the repeat region was confirmed using the R3 repeat construct [19] and tau construct lacking the R2 repeat [20]. At last, two recent studies using isothermal titration calorimetry and mass spectrometry suggested presence of additional lower-affinity sites on tau [21,22]. However, the exact location of these elusive sites remained unknown.

In this work we used a combination of Nuclear Magnetic Resonance (NMR) assays and molecular simulations to identify zinc chelating amino-acids of tau, and propose a structure for three zinc binding sites on tau protein. We pinpoint the zinc-binding residues in the high affinity binding site in the R2R3 region and uncover the existence of two novel lower affinity binding sites in N and C terminal parts of tau.

2. Materials and methods

Peptide synthesis: Synthetic pR2R3 peptide was purchased from GeneCust.

Protein expression and purification: The full-length tau and histidine mutants (H to A) were expressed from a pET-3d vector introduced into Escherichia coli BL21(DE3). After 3 h of induction with 0.5 mM isopropyl β-D-1-thiogalactopyranoside (IPTG), cells were centrifuged and the pellets were resuspended into a lysis buffer as previously described [27]. Lysis was pursued using three runs of French press at 4 tones, and non-thermostable proteins were precipitated at 95°C for 11 minutes. Then, the lysate was centrifuged at 30 000 g for 30 min at 4°C, and the supernatant was injected onto a HiTrap SP Sepharose HP cation exchange column pre-equilibrated with a 50 mM MES pH 6.5 buffer. Tau was eluted with a 50 mM MES NaCl 0.5 M pH 6.5 buffer at 1 mL/min, dialysed three times against 2 L of water at 4°C for 2 h, and dry-lyophilized. For ^{15}N labeled-tau, cells were grown on LB medium, centrifuged and

the pellet was solubilized in M9 medium containing ^{15}N ammonium chloride. Prior to use, each tau sample was airfuged at 25 psi and dosed at 280 nm with an extinction coefficient of 7700 $M^{-1}.cm^{-1}$ by spectrophotometry as previously described [27].

NMR spectroscopy: NMR spectra were recorded on a Bruker spectrometer 600 MHz equipped with a TCI cryoprobe (Triple Resonance Probe). NMR experiments (^{15}N-HSQC) were performed at 280°K (7°C) on 50 µM for ^{15}N-labeled tau samples and 1 mM for pR2R3 peptide. For the pH variations experiments, tau was resuspended into a sodium phosphate buffer at pH 6.1 and 6.7 respectively. For zinc titrations, the buffer was 20 mM MES, 100 mM NaCl, pH 6.5. Using previous chemical shift assignments, we identified the cross-peaks corresponding to the N-terminal and C-terminal extremities in the full-length tau (BMRB entry 17920 [28]) and repeat region in the pR2R3 spectrum (BMRB entry 19253 [29]). H362, H374, H388 and H407 were assigned on the tau-WT spectrum by using alanine mutants of tau. Data was processed and analyzed with TopSpin software from Bruker.

Molecular simulations: The Rosetta *de novo* structure prediction method with Monte-Carlo approach was utilized for structure prediction for tau fragments with zinc coordination restraints [30]. Fragment library was built with the Robetta web server [31] for the whole tau protein isoform hTau40 (UniProt identifier : P10636-8). This fragment library was adopted to three selected regions of tau. Simulations were started from an extended chain and then subjected to *ab initio* folding protocol with zinc coordination restraints with scoring function ref2015 [32]. Zinc incorporation was done as it was described in the original report with distance and angle restraints to the supposed coordination sphere. All backbone and sidechain torsions and zinc rigid-body degrees of freedom were optimized simultaneously in the all-atom refinement stage according to the original report [30]. For each of three Tau regions, 45,000 models were generated and the first 100 models were selected for further analysis. The top model was chosen based on the pair score.

3. Results

3.1. Localization of zinc-binding sites

Several studies have concluded that the amino acids responsible for zinc binding to tau are located in the R2R3 repeat region of tau [15,17,19,20]. More recently it was suggested that additional sites would exist most likely located outside of this repeat region [21,22]. In order to identify the zinc binding sites on tau protein, we performed ^{15}N-Heteronuclear Single Quantum Coherence (HSQC) NMR on tau in the absence and in the presence of zinc.

Since the already published amino acid assignment for the full-length tau covers only the N-terminal part and a few residues from the C-terminal part [27], we conducted three separate sets of NMR experiments. First on a R2R3 synthetic peptide, which has been previously assigned [29], thus allowing us to study the effect of zinc on the R2R3 region. Second on the full-length tau, to identify the amino acids implicated in zinc binding in the N-terminal using the previously published assignments on the full protein [28]. Finally, we used punctual tau mutants, to identify the amino acids that could interact with zinc in the C-terminal part of tau.

3.1.1. Identification of zinc binding residues in R2R3 region of tau

To first explore the R2R3 repeat domain of tau, we recorded the ^{15}N-HSQC spectrum at ^{15}N-natural abundance on pR2R3 peptide (pR2R3, Fig. 1) in the absence of zinc (Fig. 2A and Fig. S1A, orange cross peaks). Using the assignment already published for this region (Biological Magnetic Resonance Bank, BMRB, entry 19253 [29]), we identified cross-peaks corresponding to all cysteine and histidine residues in this region (C291, H299, C322, H329 and H330). In the presence of zinc (Fig. 2A and Fig S1A, blue peaks), only the cross-peaks corresponding to H299, C322, H329 and H330 were shifted, indicating that these four residues of the R2R3 region participate in the chelation of zinc in pR2R3 peptide.

3.1.2. Identification of zinc binding residues in the N-terminal region of tau

To explore the N-terminal regions of tau, first we recorded the ^{15}N-HSQC spectrum of full-length tau (Fig. 1, tau-WT, wild type) in the absence of zinc (Fig. 2B and Fig. S1B, orange peaks). Using the previously published amino-acid assignment map (BMRB, entry 17920 [28]), we identified the cross-peaks of the N-terminal part of tau, and recorded the spectrum in the presence of zinc (Fig. 2B and Fig. S1B, blue peaks).

Since the N-terminal region of tau was fully assigned, this allowed us to identify the chemical shifts for all amino acids in the presence of zinc (see Fig. S2 and Table S1). Thereby, we found four regions that were particularly impacted by zinc: a first region (11-19), where the biggest shifts were observed with M11, D13, H14, A15, G16, T17 and Y18; a second region (28-32) with G28, T30, M31 and H32; a third region (91-101) with A91, H94, E96 and T101; and finally, a fourth region (119-133) with A119, G120, H121, V122, V128 and D133. Each region contained at least one potential chelator of zinc. Indeed the first region contained one aspartate and one histidine, the second one histidine, the third one histidine and glutamate and the fourth one histidine and one aspartate. Taking into account the intrinsically disordered nature of tau, this binding site could consist of different combinations of those amino acids.

3.1.3. *Identification of zinc binding residues in the C-terminal regions of tau*

Among all of the potential zinc-chelators in the C-terminal part of tau, we distinguish 4 histidines (H362, H374, H388 and H407), 4 glutamates (E372, E380, E391, and E431) and 5 aspartates (D387, D402, D418, D421 and D430). As previously reported, histidines and cysteines are the most common residues participating in the zinc chelation spheres in proteins [33,34]. Therefore, as the C-terminal part of tau does not contain any cysteine residue, we decided to first focus on the four histidine residues of tau: H362, H374, H388, and H407. Since there was no published assignment of this region, in order to show their implication in zinc binding we generated single amino-acids mutants for each of the four histidines of this region (Fig. 1, tau-H362A, tau-H374A, tau-H388A, and tau-H407A) and

recorded ^{15}N-HSQC spectra of these mutants (see Fig. S3, orange peaks). The superimposition of the spectra of tau histidine-mutants (Fig. 3A) revealed the location of the four C-terminal histidines of tau, as one cross-peak was missing in each mutant, thus corresponding to the histidine which was mutated. The superimposition of the spectrum of each mutant with the tau-WT spectrum (Fig. S3) confirmed that all of the four cross-peaks were present in the tau-WT spectrum, but missing in the histidine-mutants spectra. This enabled us to identify the cross-peaks corresponding to H362, H374, H388 and H407 on the full-length tau spectrum (Fig. 3B, orange peaks). The addition of zinc induced a perturbation for each of these cross-peaks (Fig. 3B, blue peaks), which indicates that H362, H374, H388 and H407 could form the C-terminal binding site of tau. To confirm this hypothesis, we performed NMR on tau-H374A, in the presence of zinc (Fig. 4). We showed that in this condition the cross peaks corresponding to H362, H388 and H407 do not shift in the presence of zinc anymore, clearly demonstrating that these four histidines belong to the same C-terminal binding site. Moreover, the cross-peaks corresponding to all of the N-terminal histidines in the C-terminal histidines mutant spectra (Fig. 4) were still shifted after any of the C-terminal histidines mutations in the presence of zinc, indicating that the N-terminal binding site is independent of the C-terminal one.

3.2. Modelisation of zinc binding sites of tau

To reveal the structural features of the three zinc binding sites of tau identified in our study, we performed molecular simulation using three small tau peptides encompassing each zinc binding site. For the N-terminal, several interaction regions between full-length tau and zinc were revealed, which contain various potential zinc chelators (cysteine, histidine, glutamate and aspartate). Given that zinc is usually tetra-coordinated and that histidines are the second most common ligands of zinc in proteins after cysteines [33,34], the most probable configuration of the N-terminal would consist of H14/H32/H94/H121. N-terminal site was

modelized using Tau peptide (13-122) (Fig. 5A). Structure prediction using Rosetta revealed that zinc binding could induce the formation of short alpha helix like elements (amino acids 86-89 and 115-119), which then bring the preceding and next loops in a possible interaction (Fig. 5A). Zinc chelation geometry was restrained by simulation protocol and close to ideal, Nδ-Zn distances are 2.2 Å and Nδ-Zn-Nδ angles are about 109 degrees. Residue H94 is supported in coordination sphere by D13 in a conformation close to form H-bond with Nε atom. Formation of such interaction makes the Nδ atom more nucleophilic like in enzyme triads and thus donor acceptor interaction may become more efficient. Similarly, residue H121 is supported with E99 by forming an H-bond with Nε. While D34 is observed in proximity of H32, distance of 6 Å does not suggest a direct interaction. H14 is not supported by interaction with acid residue, the closest residue capable for H-bond formation is Y29. For the R2R3 region (Fig. 5B), we identified H299, C322, H329 and H330 as the residues chelating zinc with our NMR experiment conducted on the pR2R3 peptide. Chelator-Zn distances and angles in the resulting model were close to ideal, 2.2 Å and 109 degrees respectively. We found only one supporting interaction for H330: P312 forms a backbone in which two backbone oxygens from K311 and P312 adopt a conformation capable of accepting hydrogen from H330 Nε. H299 and H329 do not have any possible interaction candidates in proximity. For the C-terminal (Fig. 5C), we set the zinc coordination sphere according to NMR data with H362/H374/H388/H407. Chelator-Zn distances and angles in the resulting model were close to ideal, 2.2 Å and 109 degrees respectively. We found only one supporting interaction for H374: D372 forms an h-bond with Nε hydrogen.

In all three cases molecular modelisation revealed that the presence of zinc induced a more condensed conformation of tau by bringing together amino acids that would otherwise be distant. This compaction may result in a more globular shape of tau, which is in agreement with previously published Dynamic Light Scattering (DLS) data [22] showing that tau presented a lower hydrodynamic diameter in the presence of zinc. However, such compaction does not seem to be associated with significant secondary structure formation.

This is consistent with a previously published work showing that tau still exhibit a random coil conformation upon the addition of zinc [21].

4. Discussion

Despite the clinical importance of tau protein and the recent discovery of zinc ions influencing the aggregation and self-assembly of tau, the number of tau-zinc interaction sites was still under debate [21,22]. In this study we propose 12 zinc-binding amino acids corresponding to three zinc-binding sites (one in the R2R3 region, one in N-terminal and one in C-terminal part).

Among the six amino acids that have been previously suggested to participate in zinc-binding to the R2R3 region of tau [15,18–20], we pinpoint the 4 amino acids (H299, C322, H329 and H330) constituting the main zinc-binding site on R2R3 peptide, which are likely to constitute the main binding site in full-length tau. This site has been previously described as the high-affinity site (10^6 M^{-1}), as mutations of cysteines and histidines of these regions disrupted the high-affinity interaction between tau repeat regions and zinc [15]. The same study showed that zinc is able to greatly increase the formation of ThT-positive tau peptide fibrils. Moreover, it has been shown that zinc decreases the survival of tauopathy model cells [17] and neuronal cells [18] by interacting directly with at least one cysteine of tau. Our data allowed us to identify the four amino-acids responsible for this toxicity, thus providing the first molecular model of the zinc high-affinity binding site on tau.

In addition, we now describe two novel zinc binding sites in the C-terminal and N-terminal regions of tau. These sites may correspond to the low-affinity ones, previously observed with ITC experiments [22]. First, the C-terminal low-affinity binding site (H362, H374, H388 and H407) is the closest site from the R2R3 region. One explanation of its role may be linked to a previous work, which describes an interaction between the R3 and the R4 regions of tau

preventing the aggregation of a R1R3R4 tau peptide [20]. Using NMR and aggregation assays, the authors have found that zinc can disrupt this interaction by competing with specific tau amino-acids, thus enhancing the aggregation of the peptide. Given that the C-terminal site starts at the end of the R4 region of tau, zinc could potentially trigger tau aggregation by preventing such interaction between R3 and R4 repeats. Second, the N-terminal low-affinity binding site (H14, H32, H94 and H121) is located far from the two other sites. However, similarly to the C-terminal site, it could play a role in the triggering of the oligomerization process, since only high zinc concentration is able to trigger the oligomerization of tau [22], thereby highlighting the role of the low-affinity sites in this process.

Thus, the zinc concentration could be one major factor of the aggregation of tau, especially considering the importance of zinc homeostasis in physiopathology [16,35]. While in healthy cells zinc concentration is at a nanomolar scale, it can increase up to 300 micromolar in pathology [35,36]. In AD for example, intraneuronal levels of zinc in cortical cells of patients have been shown to be increased in comparison to healthy cells [37]. Similarly, high concentrations of zinc were found inside the somata and dendrites of AD neurons [38]. This accumulation may be linked to the functionality of zinc-bound proteins, which can be impaired due to alteration of neuronal metabolism in pathology [35,39,40]. Importance of zinc binding to tau has also been evoked in a physiological context, when the zinc concentrations are lower [16]. Thus, zinc binding to tau may have physiological implications with low-intraneuronal concentrations of zinc, while possibly affecting the pathological aggregation found in tauopathies at high zinc concentration [21]. The 3D models of the R2R3 site, N-terminal site and C-terminal site that we described here provide a molecular basis for future tau functionality and tau aggregation investigations, in order to decipher this mechanism that has multiple implications in neurophysiopathology.

5. Conclusion

In this study, we propose three zinc binding sites of tau protein and provide a molecular model of zinc ions binding on tau. Overall, the molecular basis of the tau-zinc interaction provided in our study will help understanding the zinc-related tau regulation or aggregation processes in both physiological and pathological conditions, thus paving the way for designing potential therapies for tauopathies.

Acknowledgements

NMR experiments were conducted in the NMR platform of IMM, Marseille, France. Molecular modelization at shared research facilities of HPC computing resources at Lomonosov Moscow State University.

References

[1] I. Sotiropoulos, M.-C. Galas, J.M. Silva, E. Skoulakis, S. Wegmann, M.B. Maina, D. Blum, C.L. Sayas, E.-M. Mandelkow, E. Mandelkow, M.G. Spillantini, N. Sousa, J. Avila, M. Medina, A. Mudher, L. Buee, Atypical, non-standard functions of the microtubule associated Tau protein, Acta Neuropathol Commun. 5 (2017). https://doi.org/10.1186/s40478-017-0489-6.

[2] Y. Wang, E. Mandelkow, Tau in physiology and pathology, Nat. Rev. Neurosci. 17 (2016) 5–21.

[3] M. Goedert, M.G. Spillantini, Propagation of Tau aggregates, Mol. Brain. 10 (2017) 18.

[4] M. Goedert, A. Klug, R.A. Crowther, Tau protein, the paired helical filament and Alzheimer's disease, J. Alzheimers. Dis. 9 (2006) 195–207.

[5] S.M. Ward, D.S. Himmelstein, J.K. Lancia, L.I. Binder, Tau oligomers and tau toxicity in neurodegenerative disease, Biochem. Soc. Trans. 40 (2012) 667–671.

[6] B. Bulic, M. Pickhardt, B. Schmidt, E.-M. Mandelkow, H. Waldmann, E. Mandelkow, Development of tau aggregation inhibitors for Alzheimer's disease, Angew. Chem. Int. Ed Engl. 48 (2009) 1740–1752.

[7] A. Ochalek, B. Mihalik, H.X. Avci, A. Chandrasekaran, A. Téglási, I. Bock, M.L. Giudice, Z. Táncos, K. Molnár, L. László, J.E. Nielsen, B. Holst, K. Freude, P. Hyttel, J. Kobolák, A. Dinnyés, Neurons derived from sporadic Alzheimer's disease iPSCs reveal elevated TAU hyperphosphorylation, increased amyloid levels, and GSK3B activation, Alzheimers. Res. Ther. 9 (2017) 90.

[8] L. Wang, Y.-L. Yin, X.-Z. Liu, P. Shen, Y.-G. Zheng, X.-R. Lan, C.-B. Lu, J.-Z. Wang, Current understanding of metal ions in the pathogenesis of Alzheimer's disease, Transl. Neurodegener. 9 (2020) 10.

[9] K. Zubčić, P.R. Hof, G. Šimić, M. Jazvinšćak Jembrek, The Role of Copper in Tau-Related Pathology in Alzheimer's Disease, Front. Mol. Neurosci. 13 (2020) 572308.

[10] W.P. Esler, E.R. Stimson, J.M. Jennings, J.R. Ghilardi, P.W. Mantyh, J.E. Maggio, Zinc-induced aggregation of human and rat beta-amyloid peptides in vitro, J. Neurochem. 66 (1996) 723–732.
[11] S. Ayala, P. Genevaux, C. Hureau, P. Faller, (Bio)chemical Strategies To Modulate Amyloid-β Self-Assembly, ACS Chem. Neurosci. 10 (2019). https://doi.org/10.1021/acschemneuro.9b00239.
[12] A.D. Efimova, R.K. Ovchinnikov, A.Y. Roman, A.V. Maltsev, V.V. Grigoriev, E.A. Kovrazhkina, V.I. Skvortsova, [The FUS protein: Physiological functions and a role in amyotrophic lateral sclerosis], Mol. Biol. (Mosk.). 51 (2017) 387–399.
[13] A. Caragounis, K.A. Price, C.P.W. Soon, G. Filiz, C.L. Masters, Q.-X. Li, P.J. Crouch, A.R. White, Zinc induces depletion and aggregation of endogenous TDP-43, Free Radic. Biol. Med. 48 (2010) 1152–1161.
[14] C. Garnier, F. Devred, D. Byrne, R. Puppo, A.Y. Roman, S. Malesinski, A.V. Golovin, R. Lebrun, N.N. Ninkina, P.O. Tsvetkov, Zinc binding to RNA recognition motif of TDP-43 induces the formation of amyloid-like aggregates, Sci. Rep. 7 (2017) 1–10.
[15] Z.-Y. Mo, Y.-Z. Zhu, H.-L. Zhu, J.-B. Fan, J. Chen, Y. Liang, Low Micromolar Zinc Accelerates the Fibrillization of Human Tau via Bridging of Cys-291 and Cys-322, J. Biol. Chem. 284 (2009) 34648–34657.
[16] Z. Xie, H. Wu, J. Zhao, Multifunctional roles of zinc in Alzheimer's disease, Neurotoxicology. 80 (2020). https://doi.org/10.1016/j.neuro.2020.07.003.
[17] Y. Huang, Z. Wu, Y. Cao, M. Lang, B. Lu, B. Zhou, Zinc Binding Directly Regulates Tau Toxicity Independent of Tau Hyperphosphorylation, Cell Rep. 8 (2014) 831–842.
[18] J.-Y. Hu, D.-L. Zhang, X.-L. Liu, X.-S. Li, X.-Q. Cheng, J. Chen, H.-N. Du, Y. Liang, Pathological concentration of zinc dramatically accelerates abnormal aggregation of full-length human Tau and thereby significantly increases Tau toxicity in neuronal cells, Biochim. Biophys. Acta. 1863 (2017) 414–427.
[19] X. Li, X. Du, J. Ni, Zn2+ Aggravates Tau Aggregation and Neurotoxicity, Int. J. Mol. Sci. 20 (2019). https://doi.org/10.3390/ijms20030487.
[20] A.C. Jiji, A. Arshad, S.R. Dhanya, P.S. Shabana, C.K. Mehjubin, V. Vijayan, Zn2+ Interrupts R4-R3 Association Leading to Accelerated Aggregation of Tau Protein, Chemistry – A European Journal. 23 (2017) 16976–16979.
[21] G.G. Moreira, J.S. Cristóvão, V.M. Torres, A.P. Carapeto, M.S. Rodrigues, I. Landrieu, C. Cordeiro, C.M. Gomes, Zinc Binding to Tau Influences Aggregation Kinetics and Oligomer Distribution, Int. J. Mol. Sci. 20 (2019) 5979.
[22] A.Y. Roman, F. Devred, D. Byrne, R. La Rocca, N.N. Ninkina, V. Peyrot, P.O. Tsvetkov, Zinc Induces Temperature-Dependent Reversible Self-Assembly of Tau, J. Mol. Biol. 431 (2019) 687–695.
[23] Y. Fichou, Y.K. Al-Hilaly, F. Devred, C. Smet-Nocca, P.O. Tsvetkov, J. Verelst, J. Winderickx, N. Geukens, E. Vanmechelen, A. Perrotin, L. Serpell, B.J. Hanseeuw, M. Medina, L. Buée, I. Landrieu, The elusive tau molecular structures: can we translate the recent breakthroughs into new targets for intervention?, Acta Neuropathol Commun. 7 (2019) 31.
[24] S. Wegmann, B. Eftekharzadeh, K. Tepper, K.M. Zoltowska, R.E. Bennett, S. Dujardin, P.R. Laskowski, D. MacKenzie, T. Kamath, C. Commins, C. Vanderburg, A.D. Roe, Z. Fan, A.M. Molliex, A. Hernandez-Vega, D. Muller, A.A. Hyman, E. Mandelkow, J.P. Taylor, B.T. Hyman, Tau protein liquid-liquid phase separation can initiate tau aggregation, EMBO J. 37 (2018). https://doi.org/10.15252/embj.201798049.
[25] V. Singh, L. Xu, S. Boyko, K. Surewicz, W.K. Surewicz, Zinc promotes liquid-liquid phase separation of tau protein, J. Biol. Chem. (2020). https://doi.org/10.1074/jbc.AC120.013166.
[26] A. Savastano, D. Flores, H. Kadavath, J. Biernat, E. Mandelkow, M. Zweckstetter, Disease-Associated Tau Phosphorylation Hinders Tubulin Assembly within Tau Condensates, Angew. Chem. Int. Ed Engl. 60 (2021) 726–730.
[27] T. De Bessa, G. Breuzard, D. Allegro, F. Devred, V. Peyrot, P. Barbier, Tau Interaction with Tubulin and Microtubules: From Purified Proteins to Cells, Methods Mol. Biol. 1523

(2017) 61–85.
[28] S. Bibow, M.D. Mukrasch, S. Chinnathambi, J. Biernat, C. Griesinger, E. Mandelkow, M. Zweckstetter, The dynamic structure of filamentous tau, Angew. Chem. Int. Ed Engl. 50 (2011) 11520–11524.
[29] P. Barré, D. Eliezer, Structural transitions in tau k18 on micelle binding suggest a hierarchy in the efficacy of individual microtubule-binding repeats in filament nucleation, Protein Sci. 22 (2013) 1037–1048.
[30] C. Wang, R. Vernon, O. Lange, M. Tyka, D. Baker, Prediction of structures of zinc-binding proteins through explicit modeling of metal coordination geometry, Protein Sci. 19 (2010) 494–506.
[31] Y. Song, F. DiMaio, R.Y.-R. Wang, D. Kim, C. Miles, T. Brunette, J. Thompson, D. Baker, High-resolution comparative modeling with RosettaCM, Structure. 21 (2013) 1735–1742.
[32] R.F. Alford, A. Leaver-Fay, J.R. Jeliazkov, M.J. O'Meara, F.P. DiMaio, H. Park, M.V. Shapovalov, P.D. Renfrew, V.K. Mulligan, K. Kappel, J.W. Labonte, M.S. Pacella, R. Bonneau, P. Bradley, R.L. Dunbrack Jr, R. Das, D. Baker, B. Kuhlman, T. Kortemme, J.J. Gray, The Rosetta All-Atom Energy Function for Macromolecular Modeling and Design, J. Chem. Theory Comput. 13 (2017) 3031–3048.
[33] S.F. Sousa, A.B. Lopes, P.A. Fernandes, M.J. Ramos, The Zinc proteome: a tale of stability and functionality, Dalton Trans. (2009) 7946–7956.
[34] M. Laitaoja, J. Valjakka, J. Jänis, Zinc Coordination Spheres in Protein Structures, Inorg. Chem. 52 (2013) 10983–10991.
[35] S.L. Sensi, P. Paoletti, A.I. Bush, I. Sekler, Zinc in the physiology and pathology of the CNS, Nat. Rev. Neurosci. 10 (2009) 780–791.
[36] X.-Y. Sun, Y.-P. Wei, Y. Xiong, X.-C. Wang, A.-J. Xie, X.-L. Wang, Y. Yang, Q. Wang, Y.-M. Lu, R. Liu, J.-Z. Wang, Synaptic released zinc promotes tau hyperphosphorylation by inhibition of protein phosphatase 2A (PP2A), J. Biol. Chem. 287 (2012) 11174–11182.
[37] D. Religa, D. Strozyk, R.A. Cherny, I. Volitakis, V. Haroutunian, B. Winblad, J. Naslund, A.I. Bush, Elevated cortical zinc in Alzheimer disease, Neurology. 67 (2006) 69–75.
[38] S.W. Suh, K.B. Jensen, M.S. Jensen, D.S. Silva, P.J. Kesslak, G. Danscher, C.J. Frederickson, Histochemically-reactive zinc in amyloid plaques, angiopathy, and degenerating neurons of Alzheimer's diseased brains, Brain Res. 852 (2000) 274–278.
[39] J.L. Smith, S. Xiong, M.A. Lovell, 4-Hydroxynonenal disrupts zinc export in primary rat cortical cells, Neurotoxicology. 27 (2006) 1–5.
[40] Tsvetkov. P.O., Roman A.Y., Baksheeva V.E, Nazipova A.A., Shevelyova. M.P., Vladimirov V.I., Buyanova. M.F., Zinchenko D.V., Zamyatnin A.A. Jr, Devred F., Golovin A.V., Permyakov S.E., Zernii E.Y., Functional Status of Neuronal Calcium Sensor-1 Is Modulated by Zinc Binding, Front. Mol. Neurosci. 11 (2018) 459–459.

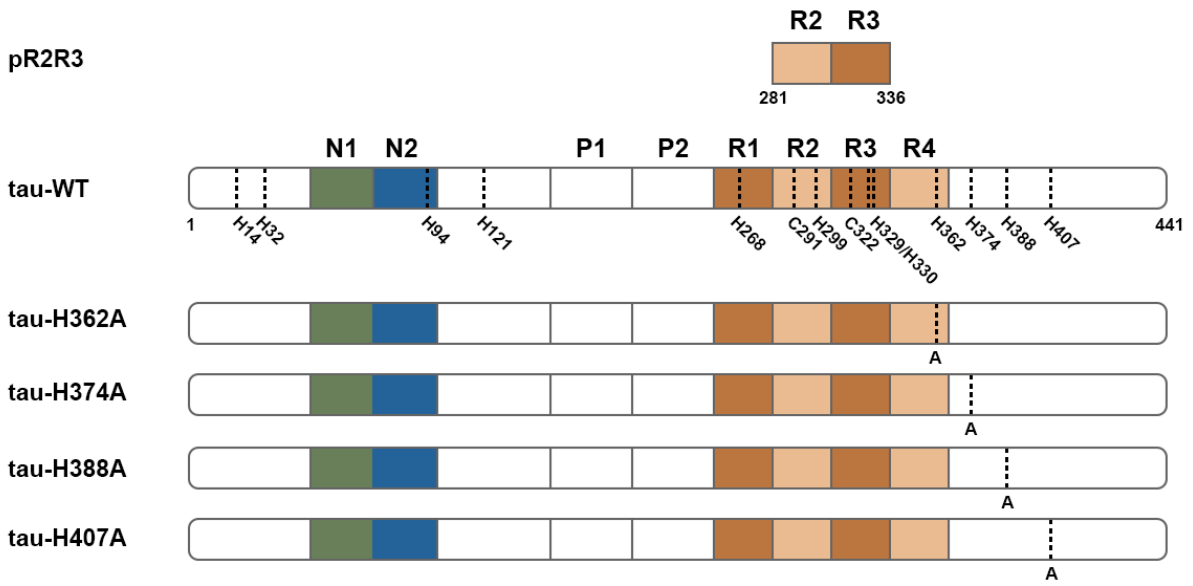

Figure 1 : Schematic representation of tau domain structure with mutations used in the study. Cysteines and histidines are represented on the tau-WT sequence, and alanine mutations for each mutant are shown below histidines positions.

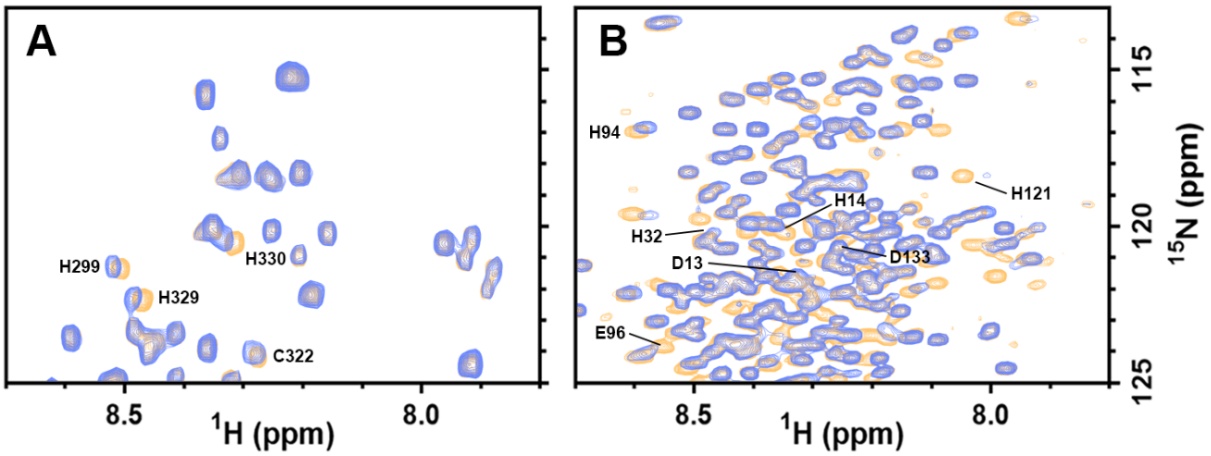

Figure 2: Binding of zinc on R2R3 tau peptide (A) and N-terminal part of tau (B). A: ^{15}N HSQC spectrum of 1 mM unlabeled pR2R3 at natural abundance in the absence (orange peaks) or in the presence of 3 mM zinc (blue peaks), highlighting the zinc chelation of R2R3 histidines and cysteines. B: ^{15}N HSQC spectrum of 50 µM ^{15}N-labeled tau-WT in the absence (orange peaks) or in the presence of 300 µM zinc (blue peaks), highlighting the zinc chelation by the N-terminal residues. All the experiments were done at 7°C to avoid aggregation in 20 mM MES 100 mM NaCl pH 6.5 unless otherwise stated.

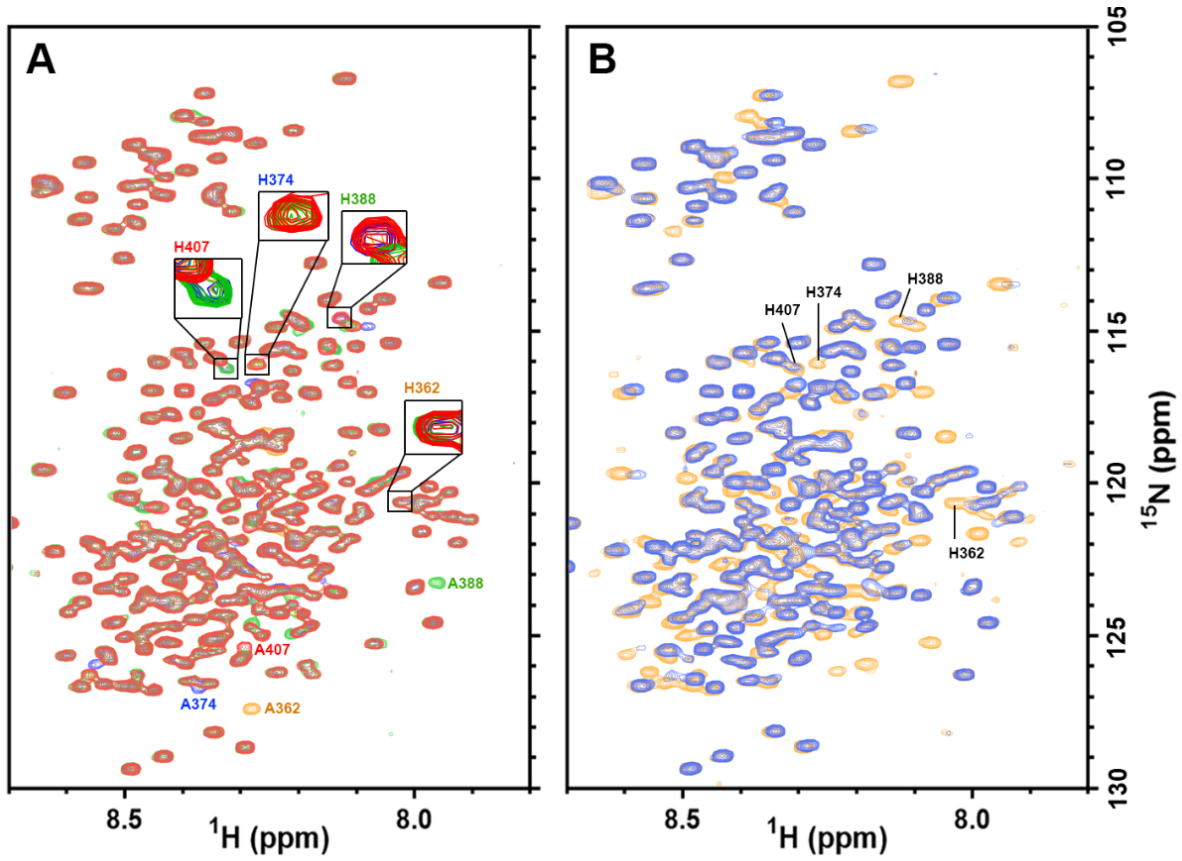

Figure 3: Identification of C-terminal histidines of tau (A) and their binding to zinc (B). A: Superimposition of histidine-mutants H362A (orange peaks), H374A (blue peaks), H388A (green peaks) and H407A (red peaks) spectra. Alanines and histidines are labeled with the same color of the corresponding spectrum. B: ^{15}N HSQC spectrum of 50 µM ^{15}N-labeled tau-WT in the absence (orange peaks) or in the presence of 300 µM zinc (blue peaks), highlighting the zinc chelation by the C-terminal histidines.

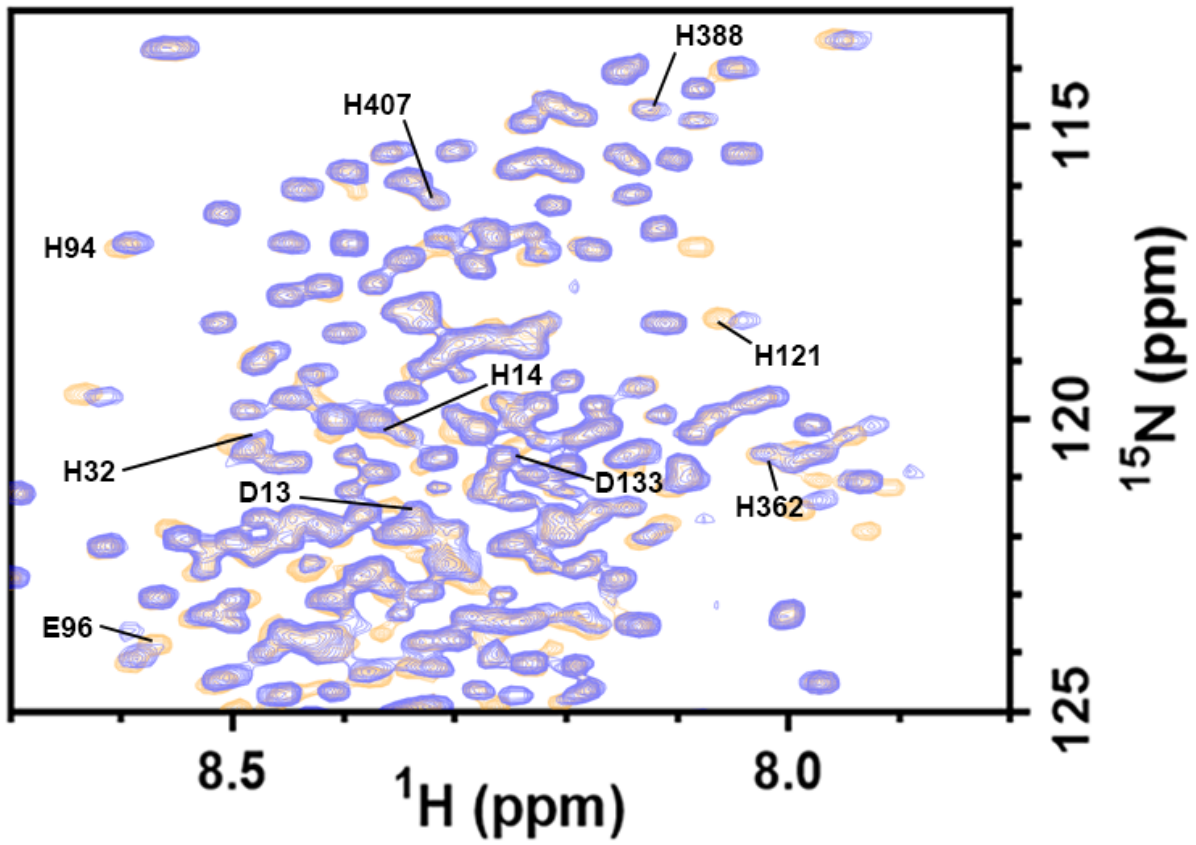

Figure 4: Effect of C-terminal histidine H374A mutation on the binding of zinc. ^{15}N HSQC spectra of tau-H374A in the absence (orange) or in the presence of zinc (blue). 50 µM of ^{15}N-labeled tau-H374A were titrated with 300 µM of zinc at 7°C. Upon H374A mutation, all of the N-terminal potential chelators (D13, H14, H32, H94, E96, H121 and D133) were still shifted upon the addition of zinc, whereas all of the cross-peaks corresponding to the C-terminal histidines were drastically affected in comparison to the experiment conducted on tau-WT (see Fig. 3B), underlying two independent sites at the N-terminal and C-terminal regions of tau.

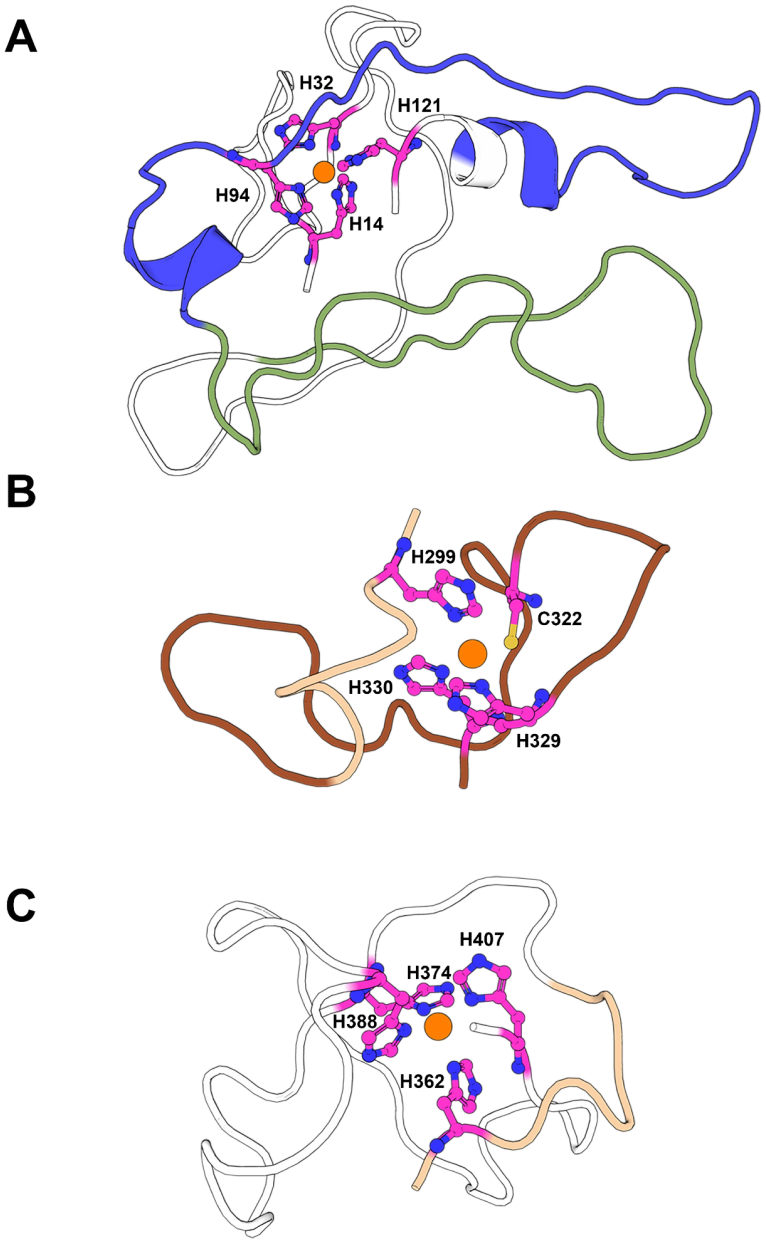

Figure 5: 3D models of the zinc-binding sites on tau. A: N-terminal (13-122), B: R2R3 (298-331) and C: C-terminal (361-408) regions of tau in the presence of zinc (orange sphere).

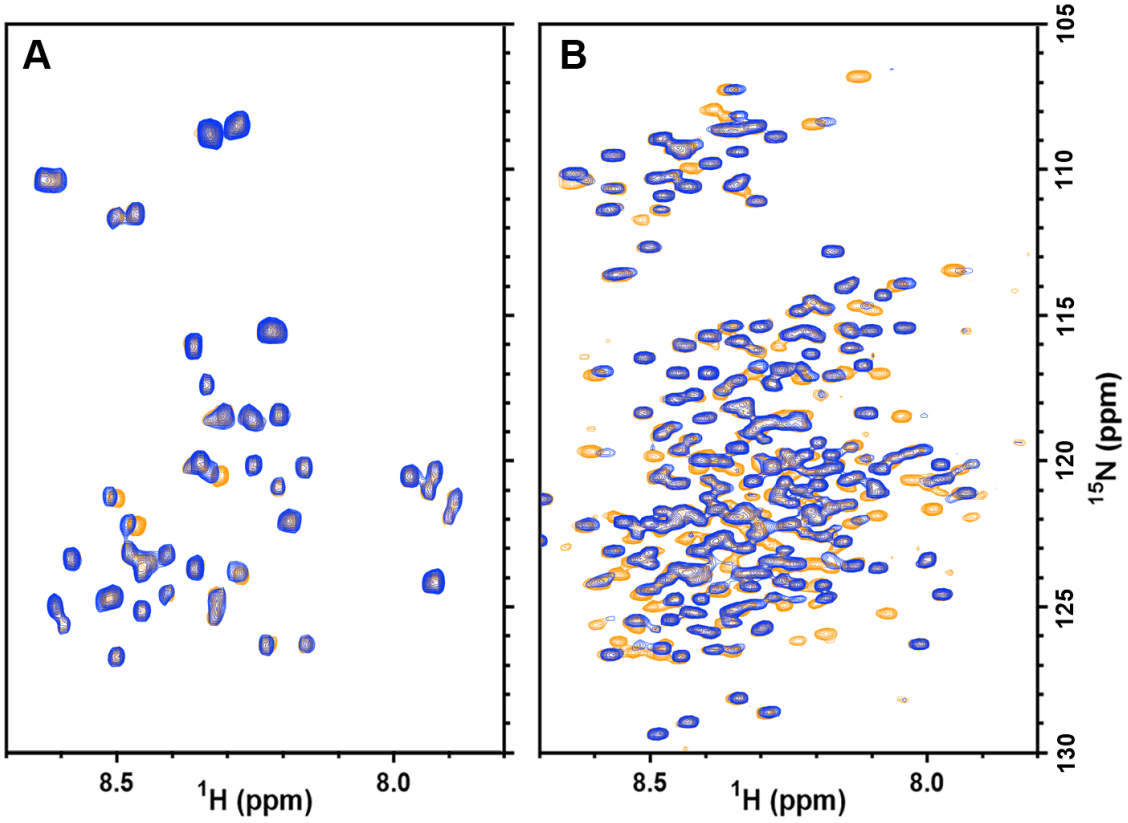

Figure S1 : ^{15}N HSQC NMR spectra of pR2R3 peptide (A) and tau-WT (B). Both of the spectra were recorded at 7°C in 20 mM MES 100 mM NaCl at pH 6.5, in the absence (orange peaks) or in the presence of zinc (blue peaks).

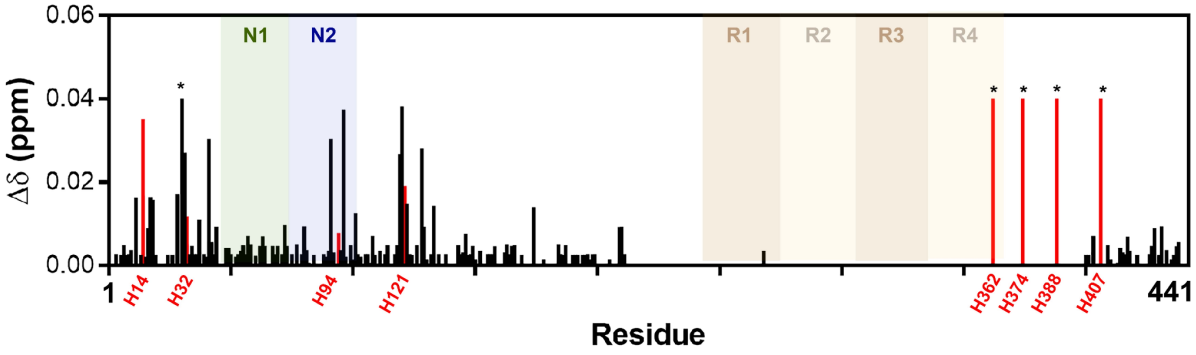

Figure S2: Shifts of each tau-WT assigned peak in the spectrum upon the addition of zinc. The residues annotated with * (T30, H362, H374, H388 and H407) did not shift but disappeared from the spectrum upon the addition of zinc, thus indicating a high perturbation.

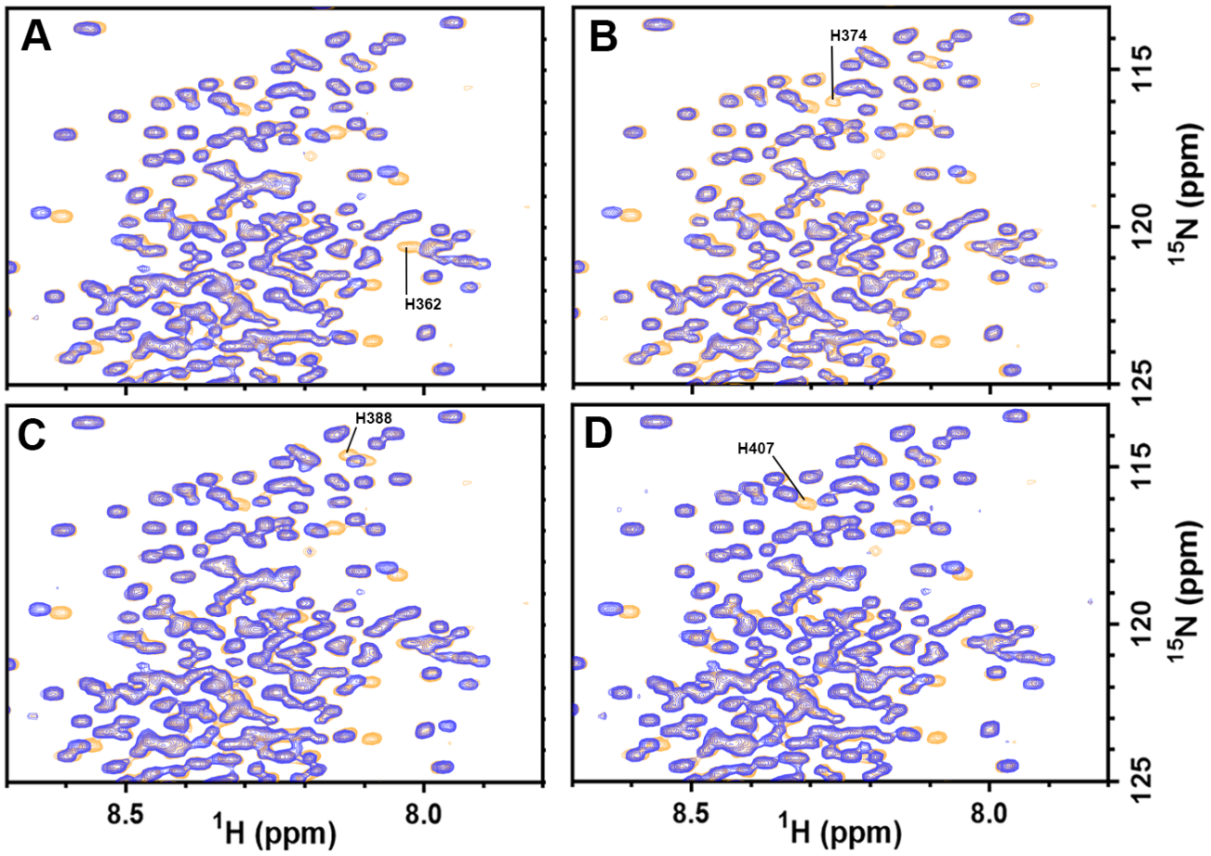

Figure S3: Superimposition of ^{15}N HSQC spectra of tau-WT and tau histidines mutants. ^{15}N HSQC spectra of tau-H362A (A), tau-H374A (B), tau-H388A (C), and tau-H407A (D) (blue) were superimposed with the tau-WT spectrum (orange). Spectra of 50 µM of ^{15}N-labeled tau-WT, tau-H362A, tau-H374A, tau-H388A and tau-H407A were recorded at 7°C.

tau-WT ppm			tau-WT ppm with zinc			Δδ (ppm)
Residue	^{1}H	^{15}N	Residue	^{1}H	^{15}N	
E3	8,669	121,199	**E3**	8,667	121,216	0,002789265
R5	8,419	121,738	**R5**	8,42	121,755	0,002505993
Q6	8,456	122,285	**Q6**	8,458	122,318	0,004876474
E7	8,429	121,978	**E7**	8,43	121,995	0,002505993
F8	8,119	119,51	**F8**	8,117	119,493	0,002789265
E9	8,236	122,324	**E9**	8,24	122,307	0,003712142
V10	8,223	122,127	**V10**	8,223	122,127	0
M11	8,498	124,606	**M11**	8,497	124,49	0,01642011
E12	8,37	121,83	**E12**	8,37	121,83	0
D13	8,313	121,667	**D13**	8,312	121,65	0,002505993
H14	8,344	120,07	**H14**	8,344	119,821	0,035213918
A15	8,31	124,287	**A15**	8,307	124,287	0,00212132
G16	8,336	108,153	**G16**	8,325	108,12	0,009070832
T17	7,924	113,403	**T17**	7,903	113,353	0,016446884
Y18	8,284	122,621	**Y18**	8,299	122,538	0,01582024
G19	8,313	110,528	**G19**	8,314	110,545	0,002505993
L20	8,07	121,089	**L20**	8,07	121,089	0
K24	8,355	121,575	**K24**	8,354	121,558	0,002505993
D25	8,322	120,173	**D25**	8,322	120,173	0
Q26	8,264	120,236	**Q26**	8,265	120,253	0,002505993
G28	8,184	108,428	**G28**	8,162	108,378	0,017088007
Y29	8,054	120,217	**Y29**	8,054	120,217	0
T30	8,055	117,044	**T30**	Disappeared		Normalized at 0,04
M31	8,258	122,882	**M31**	8,294	122,948	0,027113096
H32	8,465	120,479	**H32**	8,467	120,562	0,011822859
Q33	8,361	121,695	**Q33**	8,363	121,678	0,002789265
D34	8,524	122,054	**D34**	8,525	122,021	0,004720169
Q35	8,33	119,658	**Q35**	8,332	119,675	0,002789265
E36	8,43	121,745	**E36**	8,432	121,762	0,002789265
G37	8,407	109,96	**G37**	8,419	110,01	0,011045361
T39	8,179	114,58	**T39**	8,181	114,563	0,002789265
D40	8,359	122,769	**D40**	8,356	122,769	0,00212132
A41	8,242	124,997	**A41**	8,242	124,782	0,030405592
G42	8,332	107,206	**G42**	8,324	107,206	0,005656854
L43	7,903	121,066	**L43**	7,901	121,049	0,002789265
K44	8,231	122,275	**K44**	8,232	122,341	0,009360556
E45	8,314	121,858	**E45**	8,314	121,858	0
S46	8,456	118,938	**S46**	8,456	118,938	0
L48	8,289	122,218	**L48**	8,283	122,218	0,004242641
Q49	8,327	121,865	**Q49**	8,322	121,848	0,004275512
T50	8,28	118,738	**T50**	8,278	118,755	0,002789265
T52	8,348	115,458	**T52**	8,345	115,458	0,00212132
E53	8,502	123,437	**E53**	8,504	123,454	0,002789265
D54	8,386	122,02	**D54**	8,391	122,02	0,003535534
G55	8,466	110,247	**G55**	8,464	110,28	0,004876474
S56	8,111	115,539	**S56**	8,109	115,522	0,002789265
E57	8,509	122,647	**E57**	8,507	122,597	0,007211103
E58	8,405	123,791	**E58**	8,408	123,824	0,005126402

tau-WT ppm			tau-WT ppm with zinc			Δδ (ppm)
Residue	^{1}H	^{15}N	Residue	^{1}H	^{15}N	
G60	8,618	110,132	**G60**	8,618	110,149	0,002404163
S61	8,172	115,707	**S61**	8,172	115,707	0
E62	8,684	122,706	**E62**	8,683	122,673	0,004720169
T63	8,21	114,925	**T63**	8,211	114,875	0,007106335
S64	8,336	118,071	**S64**	8,337	118,104	0,004720169
D65	8,362	122,628	**D65**	8,362	122,628	0
A66	8,166	124,256	**A66**	8,166	124,256	0
K67	8,219	120,067	**K67**	8,22	120,1	0,004720169
S68	8,243	116,886	**S68**	8,241	116,869	0,002789265
T69	8,209	118,458	**T69**	8,208	118,491	0,004720169
T71	8,385	115,763	**T71**	8,381	115,763	0,002828427
A72	8,463	126,599	**A72**	8,459	126,533	0,009752948
E73	8,33	119,576	**E73**	8,329	119,543	0,004720169
V75	8,159	120,284	**V75**	8,161	120,301	0,002789265
A77	8,284	128,704	**A77**	8,281	128,671	0,005126402
L79	8,37	122,663	**L79**	8,368	122,68	0,002789265
V80	8,193	122,045	**V80**	8,195	122,111	0,009440339
D81	8,44	124,8	**D81**	8,444	124,783	0,003712142
E82	8,553	123,121	**E82**	8,552	123,121	0,000707107
A84	7,949	124,536	**A84**	7,95	124,519	0,002505993
K87	8,121	120,659	**K87**	8,121	120,659	0
Q88	8,377	121,25	**Q88**	8,379	121,233	0,002789265
A89	8,377	125,862	**A89**	8,374	125,862	0,00212132
A90	8,273	123,447	**A90**	8,278	123,447	0,003535534
A91	8,246	123,43	**A91**	8,246	123,215	0,030405592
Q92	8,321	120,302	**Q92**	8,318	120,285	0,003206244
H94	8,607	119,615	**H94**	8,596	119,615	0,007778175
T95	8,085	116,653	**T95**	8,112	116,156	0,072833234
E96	8,535	123,892	**E96**	8,535	123,627	0,037476659
I97	8,297	124,275	**I97**	8,294	124,275	0,00212132
E99	8,595	122,249	**E99**	8,597	122,216	0,004876474
G100	8,546	110,621	**G100**	8,548	110,621	0,001414214
T101	8,032	113,974	**T101**	8,02	113,908	0,012614278
T102	8,324	117,238	**T102**	8,322	117,221	0,002789265
A103	8,555	126,66	**A103**	8,552	126,66	0,00212132
E104	8,364	120,614	**E104**	8,364	120,614	0
E105	8,326	122,02	**E105**	8,324	122,037	0,002789265
A106	8,333	125,149	**A106**	8,335	125,166	0,002789265
G107	8,29	108,478	**G107**	8,289	108,478	0,000707107
I108	7,939	120,067	**I108**	7,941	120,117	0,007211103
G109	8,49	112,642	**G109**	8,489	112,625	0,002505993
T111	8,205	117,191	**T111**	8,2	117,191	0,003535534
S113	8,583	117,058	**S113**	8,581	117,041	0,002789265
L114	8,498	124,446	**L114**	8,496	124,413	0,004876474
E115	8,354	120,932	**E115**	8,354	120,932	0
D116	8,196	120,922	**D116**	8,196	120,922	0
E117	8,334	121,992	**E117**	8,336	121,975	0,002789265
A118	8,229	123,619	**A118**	8,227	123,652	0,004876474

tau-WT ppm			tau-WT ppm with zinc			Δδ (ppm)
Residue	^{1}H	^{15}N	Residue	^{1}H	^{15}N	
A119	7,972	121,666	**A119**	7,962	121,484	0,026692321
G120	8,102	106,778	**G120**	8,057	106,629	0,038164381
H121	8,021	118,308	**H121**	7,994	118,308	0,019091883
V122	8,079	121,957	**V122**	8,058	121,957	0,014849242
T123	8,259	118,557	**T123**	8,257	118,574	0,002789265
Q124	8,39	123,122	**Q124**	8,389	123,105	0,002505993
A125	8,402	125,26	**A125**	8,402	125,26	0
R126	8,217	119,957	**R126**	8,215	119,924	0,004876474
V128	8,385	120,27	**V128**	8,386	120,071	0,028151732
S129	8,383	120,123	**S129**	8,382	120,057	0,009360556
K130	8,405	124,04	**K130**	8,403	124,04	0,001414214
K132	8,431	123,73	**K132**	8,429	123,713	0,002789265
D133	8,216	120,445	**D133**	8,221	120,544	0,014440222
G134	8,322	109,34	**G134**	8,322	109,34	0
T135	8,138	112,732	**T135**	8,14	112,715	0,002789265
G136	8,548	111,324	**G136**	8,548	111,324	0
S137	8,219	115,63	**S137**	8,219	115,63	0
D138	8,415	122,027	**D138**	8,417	122,044	0,002789265
K141	8,071	121,235	**K141**	8,071	121,235	0
A142	8,165	124,728	**A142**	8,165	124,728	0
K143	8,295	120,624	**K143**	8,297	120,657	0,004876474
G144	8,371	109,72	**G144**	8,373	109,737	0,002789265
A145	8,274	123,733	**A145**	8,277	123,75	0,003206244
D146	8,309	118,278	**D146**	8,305	118,328	0,007615773
G147	8,243	108,824	**G147**	8,242	108,807	0,002505993
K148	8,136	120,148	**K148**	8,138	120,165	0,002789265
T149	8,196	116,421	**T149**	8,195	116,388	0,004720169
K150	8,437	125,491	**K150**	8,435	125,491	0,001414214
A152	8,471	129,378	**A152**	8,466	129,378	0,003535534
R155	8,479	122,12	**R155**	8,481	122,137	0,002789265
G156	8,419	110,508	**G156**	8,417	110,525	0,002789265
A157	8,068	123,649	**A157**	8,066	123,632	0,002789265
A158	8,317	125,146	**A158**	8,317	125,113	0,004666905
Q162	8,143	119,691	**Q162**	8,146	119,708	0,003206244
K163	8,498	123,32	**K163**	8,495	123,287	0,005126402
G164	8,443	110,239	**G164**	8,441	110,222	0,002789265
Q165	8,195	119,756	**Q165**	8,194	119,723	0,004720169
A166	8,438	125,432	**A166**	8,44	125,399	0,004876474
N167	8,395	117,676	**N167**	8,395	117,676	0
A168	8,21	124,233	**A168**	8,21	124,233	0
T169	8,125	114,055	**T169**	8,124	114,038	0,002505993
R170	8,344	120,218	**R170**	8,344	120,119	0,014000714
T175	8,248	118,762	**T175**	8,248	118,762	0
A178	8,398	125,741	**A178**	8,4	125,741	0,001414214
K180	8,436	121,985	**K180**	8,436	121,985	0
S184	8,492	116,468	**S184**	8,495	116,435	0,005126402
S185	8,441	117,889	**S185**	8,439	117,872	0,002789265
G186	8,325	110,486	**G186**	8,324	110,469	0,002505993

tau-WT ppm			tau-WT ppm with zinc			Δδ (ppm)
Residue	^{1}H	^{15}N	Residue	^{1}H	^{15}N	
E187	8,184	122,089	**E187**	8,182	122,122	0,004876474
K190	8,466	121,784	**K190**	8,465	121,767	0,002505993
S191	8,372	116,967	**S191**	8,373	116,984	0,002505993
G192	8,454	110,851	**G192**	8,453	110,834	0,002505993
R194	8,411	121,759	**R194**	8,412	121,776	0,002505993
S195	8,431	116,989	**S195**	8,432	116,972	0,002505993
G196	8,407	110,545	**G196**	8,405	110,562	0,002789265
Y197	7,953	120,629	**Y197**	7,955	120,629	0,001414214
S198	8,08	118,366	**S198**	8,078	118,35	0,002668333
S199	8,277	118,557	**S199**	8,275	118,574	0,002789265
T205	8,016	115,36	**T205**	8,014	115,36	0,001414214
R209	8,409	122,642	**R209**	8,409	122,576	0,00933381
S210	8,29	117,041	**S210**	8,289	116,975	0,009360556
R211	8,396	123,193	**R211**	8,394	123,176	0,002789265
H268	8,289	118,927	**H268**	8,289	118,927	0
H362	7,997	120,632	**H362**	Disappeared		Normalized at 0,04
H374	8,248	116,067	**H374**	Disappeared		Normalized at 0,04
H388	8,102	114,671	**H388**	Disappeared		Normalized at 0,04
V398	8,199	121,025	**V398**	8,199	121,025	0
S400	8,459	120,397	**S400**	8,458	120,414	0,002505993
G401	8,448	110,817	**G401**	8,447	110,8	0,002505993
T403	8,171	114,755	**T403**	8,169	114,705	0,007211103
R406	8,413	121,872	**R406**	8,413	121,872	0
H407	8,293	116,215	**H407**	Disappeared		Normalized at 0,04
S409	8,321	115,832	**S409**	8,319	115,865	0,004876474
N410	8,433	120,759	**N410**	8,431	120,759	0,001414214
V411	8,04	120,052	**V411**	8,04	120,052	0
S412	8,406	119,227	**S412**	8,406	119,227	0
S413	8,495	118,36	**S413**	8,496	118,36	0,000707107
T414	8,181	114,672	**T414**	8,186	114,689	0,004275512
G415	8,28	111,006	**G415**	8,277	111,023	0,003206244
S416	8,119	115,436	**S416**	8,121	115,419	0,002789265
I417	8,223	122,204	**I417**	8,223	122,254	0,007071068
D418	8,305	123,841	**D418**	8,31	123,841	0,003535534
V420	8,072	121,153	**V420**	8,072	121,153	0
D421	8,372	122,797	**D421**	8,373	122,78	0,002505993
S422	8,149	117,036	**S422**	8,149	117,036	0
A426	8,315	125,015	**A426**	8,313	124,998	0,002789265
T427	8,134	114,058	**T427**	8,133	114,091	0,004720169
L428	8,24	124,85	**L428**	8,229	124,817	0,009070832
D430	8,212	118,801	**D430**	8,213	118,818	0,002505993
E431	8,254	121,063	**E431**	8,252	120,997	0,009440339
S433	8,301	117,997	**S433**	8,305	118,014	0,003712142
A434	8,278	125,698	**A434**	8,278	125,698	0
S435	8,093	114,704	**S435**	8,091	114,704	0,001414214
L436	7,977	123,372	**L436**	7,976	123,355	0,002505993
A437	7,966	123,256	**A437**	7,966	123,289	0,004666905
K438	8,005	119,673	**K438**	7,997	119,673	0,005656854

tau-WT ppm			tau-WT ppm with zinc			Δδ (ppm)
Residue	^{1}H	^{15}N	Residue	^{1}H	^{15}N	
G440	8,313	109,363	**G440**	8,313	109,363	0
L441	7,752	126,712	**L441**	7,752	126,712	0

Supplementary Table S1: Shifts of tau-WT cross-peaks (ppm) of each residue upon the addition of zinc. All cross-peaks were identified using previously published assignments (BMRB entry 17920 [26]), and the four C-terminal histidines were assigned by identification using tau-H362A, H374A, H388A and H407A spectra as described in the main text.